BIOCHEMISTRY
including biophysical chemistry & molecular biology

Article

pubs.acs.org/biochemistry

Crystal Structures and Kinetics of Monofunctional Proline Dehydrogenase Provide Insight into Substrate Recognition and Conformational Changes Associated with Flavin Reduction and Product Release

Min Luo,[†] Benjamin W. Arentson,[‡] Dhiraj Srivastava,[†] Donald F. Becker,[‡] and John J. Tanner*[,†,§]

[†]Department of Chemistry, University of Missouri—Columbia, Columbia, Missouri 65211, United States

[‡]Department of Biochemistry, University of Nebraska—Lincoln, Lincoln, Nebraska 68588, United States

[§]Department of Biochemistry, University of Missouri—Columbia, Columbia, Missouri 65211, United States

Supporting Information

ABSTRACT: Proline dehydrogenase (PRODH) catalyzes the FAD-dependent oxidation of proline to Δ^1-pyrroline-5-carboxylate, which is the first step of proline catabolism. Here, we report the structures of proline dehydrogenase from *Deinococcus radiodurans* in the oxidized state complexed with the proline analogue L-tetrahydrofuroic acid and in the reduced state with the proline site vacant. The analogue binds against the *si* face of the FAD isoalloxazine and is protected from bulk solvent by helix α8 and the β1−α1 loop. The FAD ribityl chain adopts two conformations in the E−S complex, which is unprecedented for flavoenzymes. One of the conformations is novel for the PRODH superfamily and may contribute to the low substrate affinity of *Deinococcus* PRODH. Reduction of the crystalline enzyme−inhibitor complex causes profound structural changes, including 20° butterfly bending of the isoalloxazine, crankshaft rotation of the ribityl, shifting of α8 by 1.7 Å, reconfiguration of the β1−α1 loop, and rupture of the Arg291−Glu64 ion pair. These changes dramatically open the active site to facilitate product release and allow electron acceptors access to the reduced flavin. The structures suggest that the ion pair, which is conserved in the PRODH superfamily, functions as the active site gate. Mutagenesis of Glu64 to Ala decreases the catalytic efficiency 27-fold, which demonstrates the importance of the gate. Mutation of Gly63 decreases the efficiency 140-fold, which suggests that flexibility of the β1−α1 loop is essential for optimal catalysis. The large conformational changes that are required to form the E−S complex suggest that conformational selection plays a role in substrate recognition.

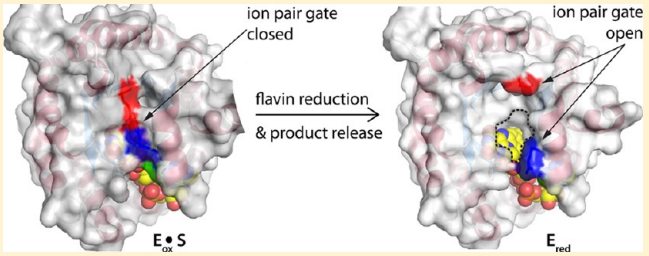

Proline dehydrogenase (PRODH) catalyzes the first reaction of proline catabolism (Figure 1A).[1] PRODH is an FAD-dependent enzyme that catalyzes the oxidation of L-proline to Δ^1-pyrroline-5-carboxylate (P5C). The electrons stored in the reduced flavin are subsequently transferred to the electron transport chain for eventual ATP production. P5C forms an equilibrium with its hydrolysis product glutamate γ-semialdehyde (GSA), which is oxidized to glutamate by the second enzyme of proline catabolism, NAD^+-dependent P5C dehydrogenase (P5CDH). PRODH and P5CDH are distinct enzymes in eukaryotes and Gram-positive bacteria, whereas the two enzymatic activities are combined into a single polypeptide chain, known as proline utilization A (PutA), in Gram-negative bacteria.[2,3]

PRODH is of interest because of its roles in apoptosis, cancer, and schizophrenia. In eukaryotes, PRODH and P5CDH are localized to the inner mitochondrial membrane and mitochondrial matrix, respectively, and proline catabolism is important for establishing the mitochondrial redox status.[4,5] Seminal work from Phang's group has established that human PRODH (also known as proline oxidase or POX) is a tumor suppressor protein.[5−13] POX expression is induced by tumor suppressor p53, and POX itself activates intrinsic and extrinsic apoptotic pathways.[8] Crucial to the role of POX as a tumor suppressor is its ability to generate superoxide.[5,8,14] Also, certain mutations in the gene encoding POX cause type I hyperprolinemia,[15] which is a risk factor for schizophrenia.[16]

Crystal structures of PRODHs suggest that conformational changes are essential for catalysis, but the details of these conformational changes have not been elucidated. We previously determined structures of the PRODH domain of *Escherichia coli* PutA (PutA86−669) complexed with proline and proline analogues,[17−19] as well as a structure of *Bradyrhizobium japonicum* PutA with a sulfate ion bound in the proline site.[20] In all of those structures, proline (or the analogue) is completely buried, implying that the active site opens to allow product release and closes again in response to

Received: September 26, 2012
Revised: November 10, 2012
Published: November 14, 2012

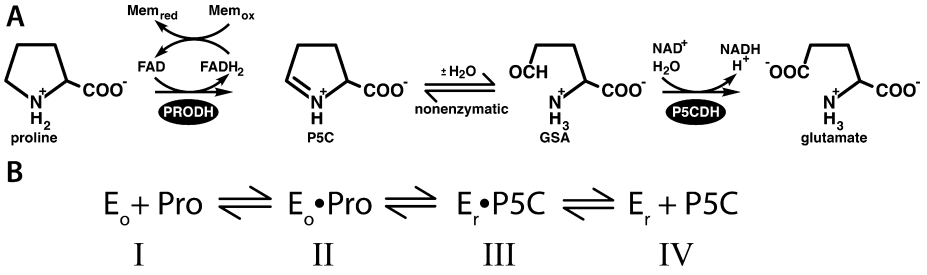

Figure 1. (A) Reactions catalyzed by PRODH and P5CDH. (B) Scheme showing the enzyme states that occur during the PRODH reductive half-reaction.

substrate binding. Because the structure of the empty PutA PRODH active site is unknown, it has not been possible to deduce these conformational changes for PutA. We also reported a structure of the monofunctional PRODH from *Thermus thermophilus* (TtPRODH) in a substrate-free conformation.[21] However, the corresponding structure of the closed, substrate-bound active site is unknown. Thus, our understanding of how conformational changes facilitate catalysis has been limited by difficulties in crystallizing the same PRODH in both the open (substrate-free) and closed (substrate-bound) conformations. Although some information has been gained by comparing the structures of PutA669-proline and ligand-free TtPRODH, this comparison is problematic because it is unknown whether PutAs and monofunctional PRODHs bind proline similarly. Another factor that complicates such a comparison is that the PRODH domain of PutA makes tertiary structural contacts that are absent in monofunctional PRODHs, and thus, it is unlikely that PutA PRODH domains and monofunctional PRODHs exhibit similar degrees of flexibility.

We therefore surveyed several monofunctional PRODHs in search of one that crystallizes in the presence of the proline analogue L-tetrahydrofuroic acid (THFA). This survey uncovered *Deinococcus radiodurans* R1 PRODH (DrPRODH) as a suitable enzyme for determining the structural changes that occur in monofunctional PRODHs during the reductive half-reaction (Figure 1B). Herein, we report high-resolution crystal structures and kinetic studies of DrPRODH, which provide new insight into substrate recognition by monofunctional PRODHs and the conformational changes that accompany flavin reduction and product release.

EXPERIMENTAL PROCEDURES

Protein Expression and Purification. The gene encoding DrPRODH (NCBI RefSeq code NP_294538.1, 310 residues) in the pMH1F vector was obtained from the Joint Center for Structural Genomics. The gene was amplified by polymerase chain reaction and ligated into plasmid pKA8H using NdeI and BamHI sites. The expressed protein includes an N-terminal His_8 tag and tobacco etch virus protease (TEVP) site. The G63A mutant of DrPRODH was created with the QuickChange II site-directed mutagenesis kit (Agilent) using a forward primer (5′-GAACCTTGACCTGCTCGCCGAATTTATCGACAGCCCG-3′) and a reverse primer (5′-CGGGCTGTCGATAAATTCCGCGAGCAGGTCAAGGTTC-3′). The E64A mutant of DrPRODH was prepared similarly using a forward primer (5′-CTTGACCTGCTCGGCGCCTTTATCGACAGCCCGGCC-3′) and a reverse primer (5′-GGCCGGGCTGTCGATAAAGGCGCCGAGCAGGTCAAG-3′). The mutations were confirmed using DNA sequencing.

DrPRODH and mutants G63A and E64A were expressed in BL21(DE3)pLysS cells as follows. Starter cultures of 10 mL were grown in LB medium overnight and used to inoculate 3 L of LB broth. After the culture had reached an optical density (OD_{600}) of 0.8, 0.5 mM IPTG was added to induce protein expression for 5 h at 22 °C. The cells were collected by centrifugation, resuspended in 50 mM Tris, 100 mM NaCl, 10 mM imidazole, and 5% glycerol (pH 7.5), and frozen at −80 °C.

DrPRODH and mutants G63A and E64A were purified as follows. The frozen cells were thawed at 4 °C in the presence of protease inhibitors (0.1 mM TPCK, 0.05 mM AEBSF, 0.1 μM pepstatin, 0.01 mM leupeptin, and 5 μM E-64) and broken using sonication. The mixture was centrifuged at 16500 rpm in an SS34 rotor for 1 h at 4 °C, filtered through a 0.45 μm filter (Millipore), and loaded into a HisTrap HP column (5 mL) that had been equilibrated in 50 mM Tris, 300 mM NaCl, 10 mM imidazole, and 5% glycerol (pH 7.5). Washing steps with the loading buffer supplemented with 10 mM imidazole followed by 30 mM imidazole were performed. The protein was eluted with 300 mM imidazole. The histidine tag was removed by incubating the protein with 0.2 mg/mL TEVP for 1 h at 28 °C followed by dialysis at 4 °C against 50 mM Tris, 50 mM NaCl, and 5% glycerol (pH 7.5). The mixture was applied to the HisTrap HP column to separate the cleaved protein, which appeared in the flow-through, from the tag and TEVP. The cleaved protein was dialyzed overnight in the dark at 4 °C into 50 mM Tris, 0.5 mM EDTA, 0.5 mM DTT, and 5% glycerol (pH 7.8) in preparation for anion exchange chromatography (HiTrap Q). The sample was loaded onto the column using a buffer consisting of 50 mM Tris and 5% glycerol (pH 7.8), and a linear NaCl gradient was applied. DrPRODH eluted in the range of 360−420 mM NaCl. The protein concentration was estimated using the bicinchoninic acid method (Pierce kit) with bovine serum albumin as the standard. The flavin contents of the purified mutants G63A and E64A were similar to that of DrPRODH.

Crystallization and Crystal Soaking Experiments. All crystallization experiments were performed at 22 °C using the sitting-drop method of vapor diffusion with drops formed by mixing equal volumes of the reservoir and the protein stock solutions. The latter solution consisted of 2.8 mg/mL DrPRODH in 50 mM Tris, 50 mM NaCl, 0.5 mM THP, 0.5 mM EDTA, 5% glycerol, and 400 mM THFA (pH 7.5). Initial conditions were identified using commercially available crystal screens (Hampton Research). Optimized crystals were grown using a reservoir solution of 0.2 M $MgCl_2$, 25% (w/v) PEG 3350, and 0.1 mM Bis-Tris (pH 5.8). The crystals were cryoprotected with the reservoir solution supplemented with 25% (v/v) PEG 200, picked up with Hampton loops, and flash-

dx.doi.org/10.1021/bi301312f | *Biochemistry* 2012, 51, 10099−10108

cooled in liquid nitrogen. The space group is $P2_12_12_1$ with the following unit cell dimensions: a = 44 Å, b = 95 Å, and c = 136 Å. The asymmetric unit includes two enzyme−THFA complexes and 40% solvent.

Crystals of DrPRODH with the FAD reduced (DrPRODH$_r$) were obtained by soaking the aforementioned crystals for ∼17 min in 50 mM sodium dithionite, 0.2 M $MgCl_2$, 25% PEG 3350, 0.1 mM Bis-Tris (pH 5.5), and 25% PEG 200. The crystal changed from deep yellow to colorless during soaking, which is consistent with reduction of the FAD. The crystals were flash-cooled in liquid nitrogen to trap the reduced enzyme conformation.

X-ray Diffraction Data Collection, Processing, and Refinement. Diffraction data were collected on beamlines 4.2.2 of the Advanced Light Source and 24-ID-C of the Advanced Photon Source. The reflections were integrated with XDS[22] and scaled with SCALA[23] (Table 1). The phase problem was solved using molecular replacement as implemented in MOLREP.[24] The search model was the $(\beta\alpha)_8$ barrel of *T. thermophilus* PRODH (residues 37−279 of chain A of Protein Data Bank (PDB) entry 2G37, 47% identical to DrPRODH). The correct solution had a correlation coefficient of 0.36 with two molecules in the $P2_12_12_1$ asymmetric unit. For reference, molecular replacement calculations that assumed other primitive orthorhombic space groups yielded correlation coefficients of 0.26−0.31. The model from molecular replacement was used as the starting point for several rounds of model building with COOT[25] and refinement with PHENIX.[26] Table 1 lists refinement statistics.

The oxidized flavin exhibits two conformations in the THFA complex (Figure S1 of the Supporting Information). The two conformations have occupancies of 0.56 (conformation A) and 0.44 (conformation B) and differ in the orientations of the 2′- and 3′-hydroxyl groups of the ribityl chain. Justification for building two conformations was obtained by refining the structure with single conformations of the FAD. For example, the $F_o - F_c$ map calculated after a refinement that included only conformation A at an occupancy of 1.0 showed strong features for the 2′-OH and 3′-OH ribityl groups of conformation B (Figure S1 of the Supporting Information, blue cage). Conversely, the map calculated after a refinement that included just conformation B at an occupancy of 1.0 showed strong features for the 2′-OH and 3′-OH ribityl groups of conformation A (Figure S1 of the Supporting Information, green cage).

Enzyme Activity Assays. All chemicals used during kinetic characterization were purchased from Fischer Scientific or Sigma-Aldrich. All steady-state assays were conducted at 23 °C in 50 mM potassium phosphate and 25 mM NaCl (pH 7.5). For all assays, coenzyme Q1 (CoQ1) was used as the electron acceptor with CoQ1 reduction monitored by the decrease in absorbance at 278 nm using a molar extinction coefficient of 14.5 mM^{-1} cm^{-1}.[27] The K_m for proline and the k_{cat} for wild-type DrPRODH (0.25 μM) were determined by varying the concentration of proline (0−500 mM) while keeping the CoQ1 concentration constant (200 μM). Inhibition of wild-type DrPRODH (0.25 μM) by THFA was analyzed by varying the proline (10−500 mM) and THFA (0−200 mM) concentrations while keeping the CoQ1 concentration constant (200 μM). These assays were performed in a total volume of 200 μL per assay using a Powerwave XS microplate spectrophotometer (Bio-Tek). The K_m for CoQ1 and the k_{cat} for wild-type DrPRODH (0.25 μM) were determined by varying the CoQ1 concentration (0−450 μM) and keeping the proline concentration constant (500 mM). For the DrPRODH mutants G63A (11 μM) and E64A (6.3 μM), the K_m for proline and the k_{cat} were determined by varying the proline concentration (0−1000 mM) and holding the CoQ1 concentration constant (200 μM). The K_m for CoQ1 and the k_{cat} for the DrPRODH mutants were determined by varying the CoQ1 concentration (10−450 μM) and holding the proline concentration constant (500 mM). These assays were performed in a total volume of 150 μL by mixing enzyme and substrate solutions using a Hi-Tech Scientific SF-61DX2 stopped-flow instrument equipped with a 0.15 cm path length cell. Steady-state parameters were

Table 1. X-ray Diffraction Data Collection and Refinement[a]

	DrPRODH$_o$−THFA	DrPRODH$_r$
FAD redox state	oxidized	reduced
space group	$P2_12_12_1$	$P2_12_12_1$
unit cell parameters (Å)	a = 44.5, b = 95.5, c = 136.4	a = 43.4, b = 95.7, c = 136.0
wavelength (Å)	0.979	1.00
resolution (Å)	95.5−1.36 (1.43−1.36)	47.8−1.75 (1.84−1.75)
no. of observations	450935	415890
no. of unique reflections	124272	58089
$R_{merge}(I)$	0.032 (0.431)	0.065 (0.837)
$R_{meas}(I)$	0.043 (0.576)	0.071 (0.905)
$R_{pim}(I)$	0.021 (0.294)	0.026 (0.341)
mean I/σ	17.1 (2.4)	22.1 (2.5)
completeness (%)	98.9 (98.5)	100.0 (100.0)
multiplicity	3.6 (3.7)	7.2 (7.0)
no. of protein residues	562	550
no. of atoms	5091	4557
no. of FAD atoms	212	106
no. of THFA atoms	16	0
no. of water molecules	475	297
R_{cryst}	0.148 (0.239)	0.182 (0.276)
R_{free}[b]	0.181 (0.279)	0.213 (0.323)
rmsd for bond lengths (Å)[c]	0.015	0.013
rmsd for bond angles (deg)	1.75	1.45
Ramachandran plot[d]		
favored (%)	99.3	99.3
allowed (%)	0.7	0.7
outliers (%)	0.0	0.0
average B (Å^2)		
protein	21.4	28.6
FAD	17.7	23.7
THFA	17.5	not applicable
acetate	not applicable	26.2
water	31.5	31.4
coordinate error (Å)[e]	0.14	0.19
PDB entry	4H6Q	4H6R

[a]Values for the outer resolution shell of data are given in parentheses. [b]A common test set (5%) was used for refinement of both structures. [c]Compared to the parameters of Engh and Huber.[34] [d]The Ramachandran plot was generated with RAMPAGE.[35] [e]Maximum likelihood-based coordinate error estimate.

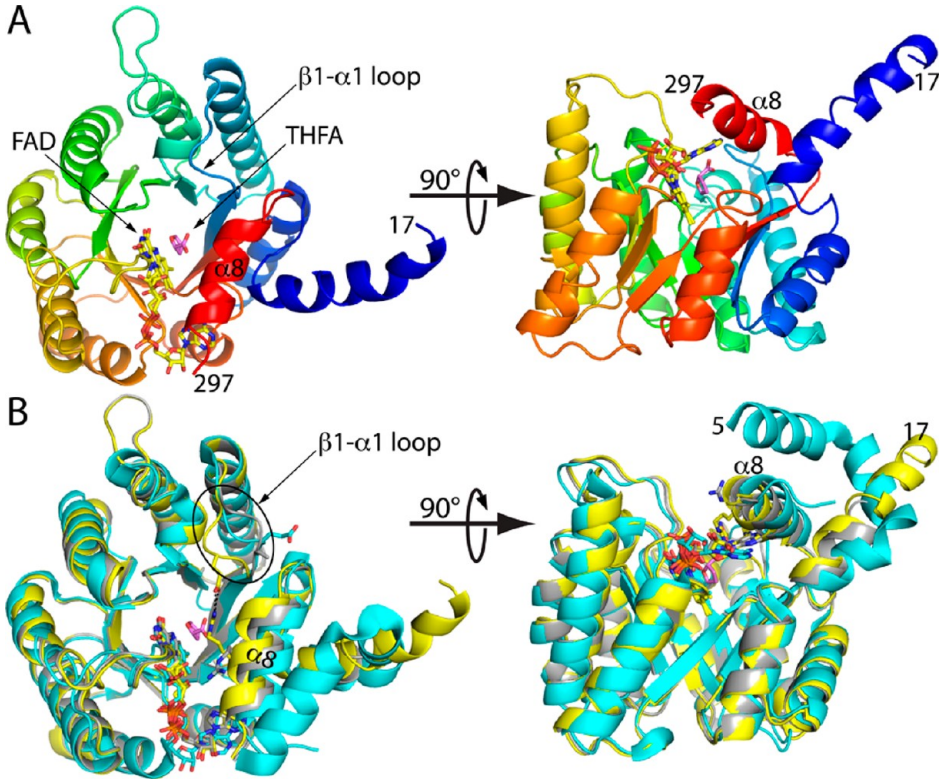

Figure 2. Overall fold of PRODH. (A) Two views of the DrPRODH$_o$–THFA structure. The backbone is colored according to a rainbow scheme, with blue at the N-terminus and red at the C-terminus. FAD is colored yellow. THFA is colored pink. Residue numbers of the N- and C-termini are noted. (B) Superposition of the DrPRODH$_o$–THFA complex (yellow), DrPRODH$_r$ (gray), and TtPRODH (cyan, PDB entry 2g37). The R291–E64 ion pair is observed only in the DrPRODH$_o$–THFA structure. This figure and others were prepared with PyMOL.[36]

calculated by fitting initial rate data to the Michaelis–Menten equation, and inhibition data were globally fit to a competitive inhibition model using Enzyme Kinetic Wizard (SigmaPlot 12.0).

RESULTS

Structure of the DrPRODH$_o$–THFA Complex. The crystal structure of oxidized DrPRODH (DrPRODH$_o$) complexed with the proline analogue THFA was determined at 1.36 Å resolution (Table 1). It is the first structure of a monofunctional PRODH complexed with a proline analogue and the highest-resolution structure of any PRODH or PutA.

The DrPRODH$_o$–THFA complex exhibits a distorted $(\beta\alpha)_8$ barrel fold in which the last helix, denoted α8 (residues 285–295), is located above the C-terminal ends of the strands rather than alongside β8 as in the classic triosephosphate isomerase barrel (Figure 2A). This fold is also observed in the structures of TtPRODH (Figure 2B) and PutA and is considered to be a defining characteristic of the PRODH superfamily, which includes both monofunctional PRODHs and PutAs. The root-mean-square deviation between the DrPRODH$_o$–THFA complex and TtPRODH is 1.2 Å; the variation from PutA PRODH domains is slightly higher, 1.5–1.9 Å.

THFA binds between the *si* face of the FAD and α8 (Figure 2A). Arg291, Arg292, and Lys98 form ion pairs with the carboxylate of THFA, while Leu257, Tyr278, and Tyr288 provide hydrophobic contacts with the pyrrolidine ring (Figure 3A). Arg291 and Arg292 are stabilized by ion pairs with Glu64 and Glu295, respectively. The plethora of residues clustered around THFA make the inhibitor and the *si* face of the flavin inaccessible to solvent.

The oxidized flavin exhibits two conformations, which is unprecedented for PRODHs and PutAs (Figure 4A). Furthermore, we are unaware of another flavin oxidoreductase that exhibits multiple flavin conformations in the E–S complex. The two conformations have occupancies of 0.56 (conformation A) and 0.44 (conformation B). Interestingly, the two FAD conformations do not correspond to THFA-bound and THFA-free states because the occupancy of THFA is clearly 1.0 (*B* factor = 17.5 Å^2). Rather, the enzyme is able to bind THFA using either of two different FAD conformations.

The two FAD conformations differ in the orientations of the 2′- and 3′-hydroxyl groups of the ribityl chain (Figure 4A and Figure S1 of the Supporting Information). In conformation A (yellow in Figure 4A), the 2′-OH points toward the proline binding site while the 3′-OH is oriented 180° away and interacts with the carbonyl of Gly191. Conformation B is related to conformation A by a crankshaft rotation around the C2′–C3′ bond. In conformation B (pink in Figure 4A), the 2′-OH is tucked under the pyrimidine ring where it forms hydrogen bonds with the flavin N1 atom and NH group of Gly191, while the 3′-OH interacts with Glu295 of α8.

Ribityl conformation A appears to be unique among the PRODH superfamily. Although it resembles the ribityl of the PutA86–669–THFA complex in that the 2′-OH points into the proline site, the other two hydroxyl groups of conformation A are rotated 180° from the corresponding hydroxyls of the PutA86–669–THFA complex (Figure 5A). Although the 4′-OH of DrPRODH overlaps the 3′-OH of the PutA86–669–THFA complex (Figure 5A), the two hydroxyls are non-equivalent because they form different interactions. The 3′-OH of the PutA86–669–THFA complex forms a hydrogen bond

dx.doi.org/10.1021/bi301312f | *Biochemistry* 2012, 51, 10099–10108

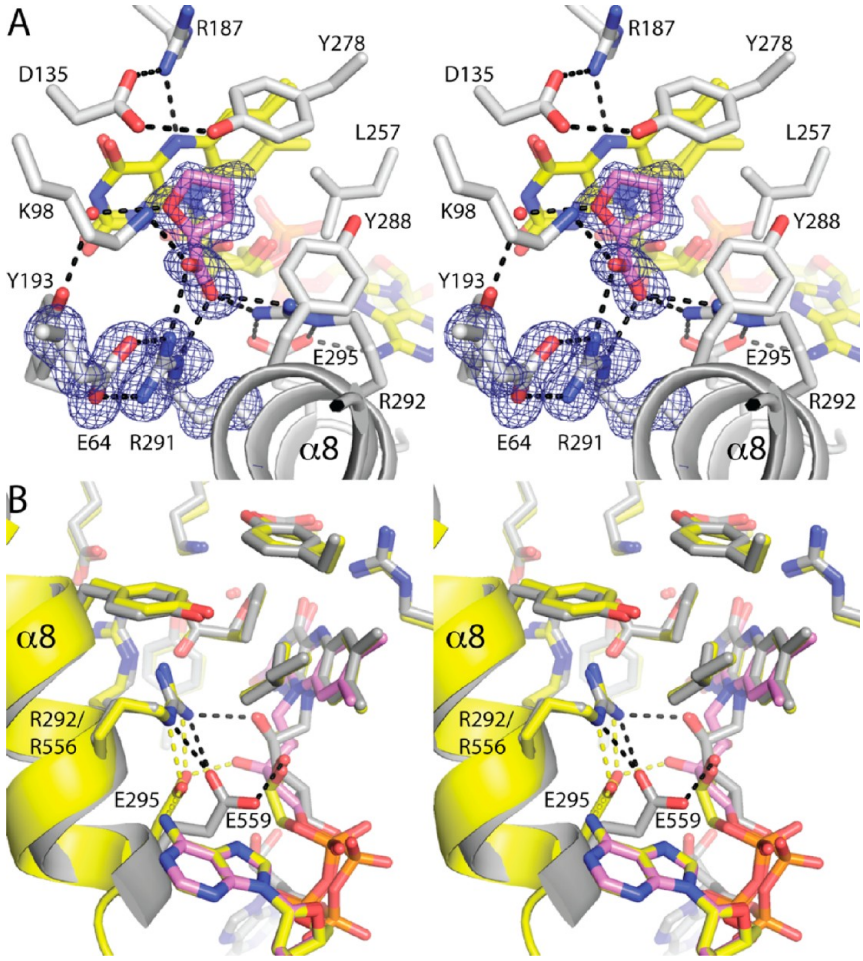

Figure 3. Active site of the DrPRODH$_o$–THFA complex (relaxed stereographic views). (A) Electron density map for the DrPRODH$_o$–THFA complex. The cage represents a simulated annealing σ_A-weighted $F_o - F_c$ omit map (3.0σ). (B) Superposition of the DrPRODH$_o$–THFA complex (yellow) and the PutA86–669–THFA complex (gray, PDB entry 1tiw), highlighting differences in the orientation of the conserved glutamate of α8 (Glu295 in DrPRODH, Glu559 in PutA). Yellow and black dashes denote the unique electrostatic interactions of DrPRODH and PutA86–669, respectively. Conformations A and B of the FAD in the DrPRODH$_o$–THFA complex are colored yellow and pink, respectively.

with the conserved Glu559 of α8 (Figure 3B), which corresponds to Glu295 of DrPRODH. Glu295, however, adopts a different conformation and is thus unable to form an analogous hydrogen bond with the 4′-OH (Figure 3B).

Ribityl B is more familiar. It is similar to the ribityl of ligand-free TtPRODH (Figure 5B). In both structures, the 2′- and 3′-hydroxyls are below the pyrimidine ring, while the 4′-OH is below the dimethylbenzene ring. One notable difference is that the 4′-OH of DrPRODH ribityl B is located on the *si* face of the FAD, whereas that of TtPRODH is torsioned over to the *re* side. The *re* side location allows the hydroxyl to engage a structurally conserved water molecule that bridges the main chains of β5 and β6 in all PRODH and PutA structures (Figure 5B).

The flavins of DrPRODH and PutA also differ in the position of the adenosine group (Figure 5A). Because of a rotation around the pyrophosphate, the adenine ring positions of the two structures differ by 13 Å. This difference was also noted in TtPRODH and is caused by the presence of an extra α-helix in PutAs that is absent in monofunctional PRODHs.[21]

Structure of DrPRODH$_r$. A 1.75 Å resolution structure of DrPRODH$_r$ was determined from a crystal of the DrPRODH$_o$–THFA complex that was soaked in sodium dithionite. Reduction causes large conformational changes in the flavin, which are observed in both molecules in the asymmetric unit. Large protein conformational changes are also observed in chain A of the asymmetric unit, and the electron density map is consistent with release of THFA. In the other chain, crystal contacts prevent large protein conformational changes, and the electron density map suggests that an acetate ion replaces THFA. We note that PutA86–669 crystallized in PEG 3350 also has an acetate ion bound in the active site.[28] The discussion below focuses on chain A, because it provides information about conformational changes in both the flavin and the protein.

Reduction by dithionite induces substantial conformational changes in the flavin. The reduced flavin exhibits a 20° butterfly bend in the isoalloxazine (Figure 4C), which contrasts the planar isoalloxazine of the oxidized enzyme. Severe butterfly bending (20–30°) has also been observed in the dithionite-reduced flavin of PutA86–669[28] and the covalently modified, reduced flavins of *N*-propargylglycine-inactivated PRODH[29] and PutA.[30] The bending of the flavin pushes the N5–N10 axis toward the proline binding site, which results in the *si* face being convex. The reduced flavin of DrPRODH$_r$ exhibits just one ribityl conformation (Figure 4B), which is nearly identical to the ribityl chains of the oxidized FAD in TtPRODH and the

dx.doi.org/10.1021/bi301312f | *Biochemistry* 2012, 51, 10099–10108

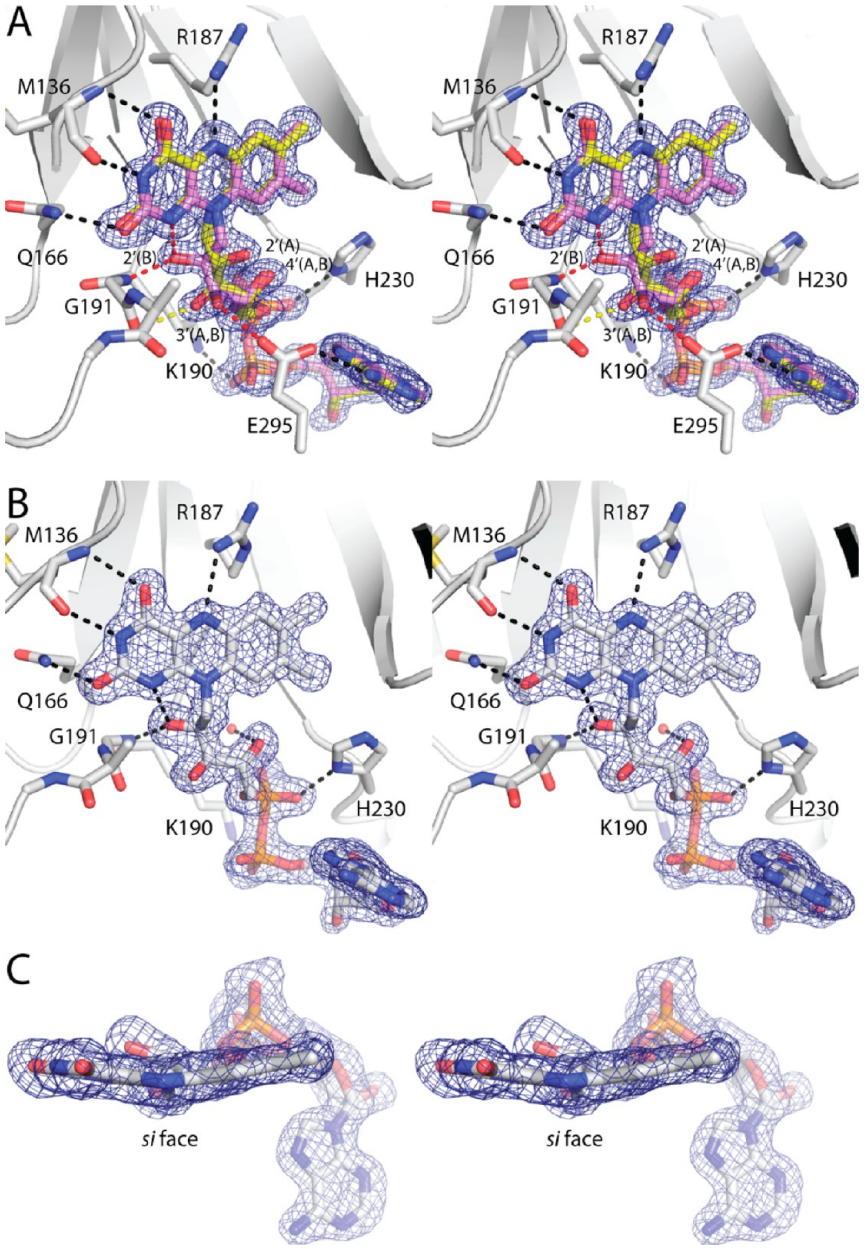

Figure 4. Conformations of the flavin in DrPRODH (relaxed stereographic views). (A) Dual FAD conformations of the DrPRODH$_o$–THFA complex. Conformations A (q = 0.56) and B (q = 0.44) are colored yellow and pink, respectively. Yellow and red dashes denote the unique hydrogen bonds of conformations A and B, respectively. Note that the two conformations differ mainly in the orientations of the 2′-OH and 3′-OH groups of the ribityl. (B and C) Two views of the dithionite-reduced flavin of DrPRODH$_r$. In all three panels, the cage represents a simulated annealing σ_A-weighted $F_o - F_c$ omit map (3.0σ).

reduced flavin in the *N*-propargylglycine-inactivated *E. coli* PutA PRODH domain[30] (Figure 5C).

Flavin reduction also dramatically changes the protein conformation. Upon flavin reduction, α8 shifts away from the isoalloxazine by 1.7 Å, and the β1–α1 loop (residues 62–69) withdraws from the active site by >5 Å (Figure 6A). One major consequence of these movements is the rupture of the Arg291–Glu64 ion pair, which links α8 and the β1–α1 loop in the THFA complex. The electron density for the ion pair in the THFA complex is exceptional, indicating that this interaction is quite strong (Figure 3A). Its rupture is thus a significant event. Breaking of the ion pair causes Glu64 and Arg291 to separate from each other. Glu64 is driven to the protein surface along with the rest of the β1–α1 loop (Figures 2B and 6A), although we note that electron density for the β1–α1 loop is relatively weak in DrPRODH$_r$, implying high mobility. In fact, density for the side chain of Glu64 in DrPRODH$_r$ is absent, indicating that the side chain is disordered. Electron density for the side chain of Arg291 is likewise weak but suggests that the guanidinium group turns away from the proline binding site (Figure 6A). Flavin reduction also induces disorder in another key side chain of α8, Glu295, which hydrogen bonds with the FAD adenine and ribityl groups in the THFA complex.

The large movements of α8 and the β1–α1 loop dismantle the proline binding site and profoundly change the solvent accessibility of the flavin. In the THFA complex, the isoalloxazine and THFA are buried beneath the Arg291–Glu64 ion pair (Figure 6B), and the interaction between

dx.doi.org/10.1021/bi301312f | *Biochemistry* 2012, 51, 10099–10108

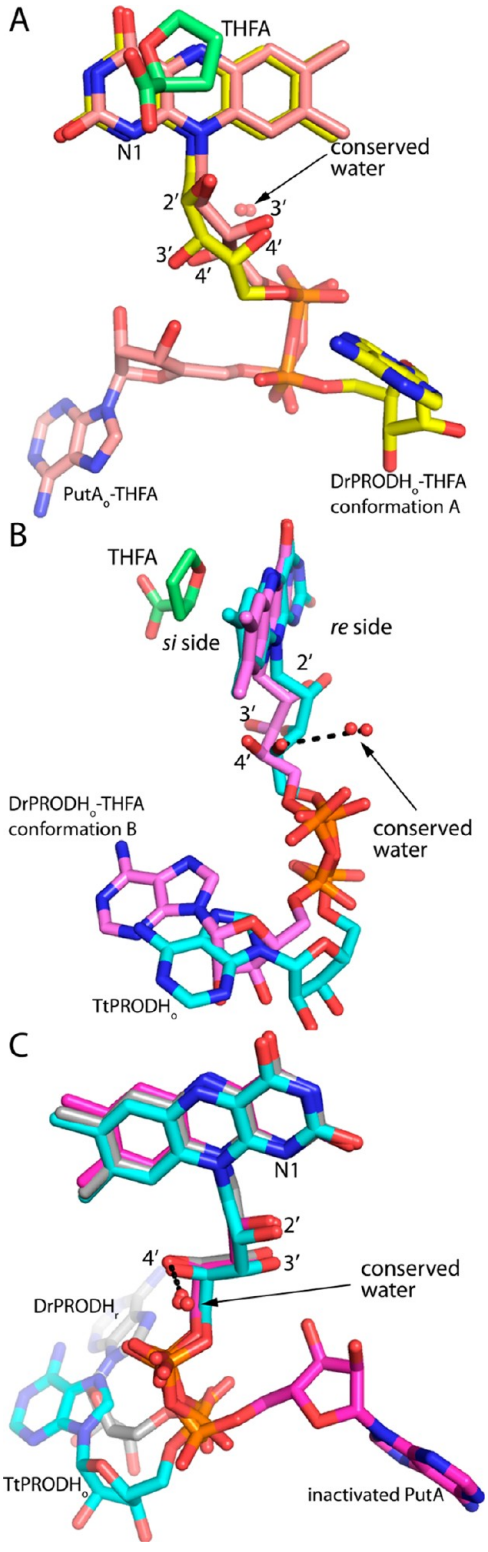

Figure 5. Comparison of flavin conformations in PRODHs and PutAs. (A) Superposition of FAD conformation A of the DrPRODH$_o$–THFA complex (yellow) and the FAD of the PutA86–669–THFA complex (salmon, PDB entry 1tiw). (B) Superposition of FAD conformation B of the DrPRODH$_o$–THFA complex (pink) and the oxidized flavin of TtPRODH (cyan, PDB entry 2g37). (C) Superposition of the reduced flavin of DrPRODH$_r$ (gray), the oxidized FAD of TtPRODH (cyan), and the inactivated flavin of the PutA PRODH domain (magenta, PDB entry 3ITG).

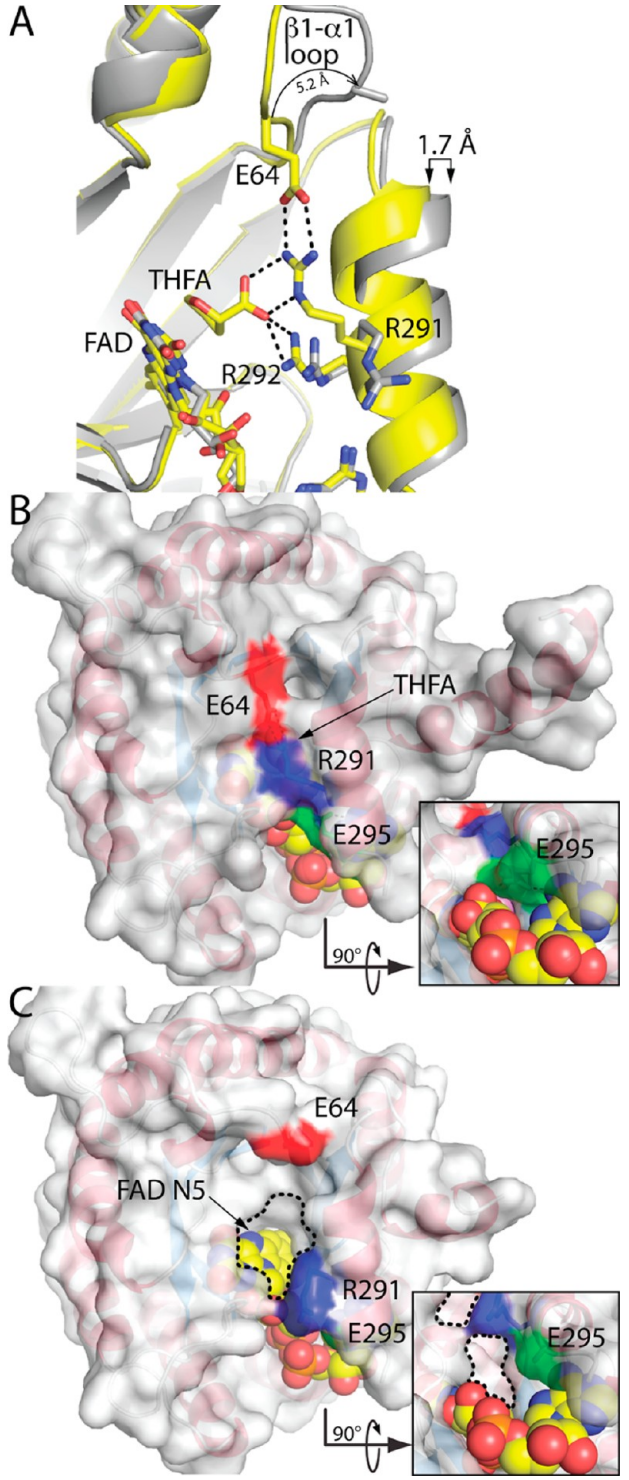

Figure 6. Conformational changes induced by flavin reduction and product release. (A) Superposition of the active sites of the DrPRODH$_o$–THFA complex (yellow) and DrPRODH$_r$ (gray) highlighting the shift of α8, reconfiguration of the β1–α1 loop, and breaking of the Arg291–Glu64 ion pair. Black dashes indicate electrostatic interactions in the DrPRODH$_o$–THFA complex. (B) Surface representation of the DrPRODH$_o$–THFA complex. FAD and THFA are drawn as yellow and pink spheres, respectively. Glu64 and Arg291 are colored red and blue, respectively. Glu295 is colored green. The inset shows a view from the bottom of the active site. (C) Surface representation of DrPRODH$_r$. The coloring is the same as in panel B. The dashes outline the openings to the active site.

dx.doi.org/10.1021/bi301312f | *Biochemistry* 2012, 51, 10099–10108

Table 2. Kinetic Parameters for DrPRODH and DrPRODH Mutant Enzymes Using Proline and CoQ1 as the Substrates

	k_{cat} (s^{-1})	K_m (mM)	k_{cat}/K_m (s^{-1} M^{-1})	variational effect (k_{cat}/K_m of mutant)/(k_{cat}/K_m of DrPRODH)
		Proline as the Variable Substrate[a]		
DrPRODH	8.7 ± 0.58	290 ± 39	30 ± 4.5	
G63A	0.080 ± 0.006	384 ± 68	0.21 ± 0.04	0.007 ± 0.002
E64A	0.055 ± 0.001	50 ± 6	1.1 ± 0.13	0.037 ± 0.007
		CoQ1 as the Variable Substrate[b]		
DrPRODH	14 ± 1	0.155 ± 0.04	90323 ± 24185	
G63A	0.043 ± 0.003	0.028 ± 0.01	1535 ± 559	0.017 ± 0.008
E64A	0.046 ± 0.003	0.032 ± 0.01	1438 ± 458	0.016 ± 0.007

[a]The CoQ_1 concentration was fixed at 200 μM. [b]The proline concentration was fixed at 500 mM.

Glu295 and the ribityl seals the bottom of the active site (Figure 6B, inset). In the reduced enzyme, the separation of Arg291 from Glu64 creates a large, solvent-exposed cavity in the upper part of the active site, which contains the isoalloxazine (Figure 6C). Furthermore, the combination of disorder in Glu295 and the change in the ribityl conformation creates a hole in the bottom of the active site of the reduced enzyme (Figure 6C, inset). Thus, the active site of the reduced, ligand-free enzyme is open, and the flavin is highly solvent exposed.

Kinetic Parameters of DrPRODH and DrPRODH β1−α1 Loop Mutants. The observation of large conformational changes in the β1−α1 loop induced by flavin reduction and release of THFA prompted an investigation of this loop using site-directed mutagenesis. As described by White et al., the β1−α1 loop harbors one of nine conserved sequence motifs that define the PRODH superfamily.[21] This motif includes a Gly-Glu pair that is present in all monofunctional PRODHs and PutAs and corresponds to the Gly63-Glu64 pair of DrPRODH. These residues were therefore investigated by creating the site-directed mutant enzymes G63A and E64A.

The kinetic parameters for wild-type DrPRODH were first determined (Table 2). The values of k_{cat} and K_m using proline as the variable substrate with a fixed CoQ1 concentration are 8.7 s^{-1} and 290 mM, respectively, resulting in a k_{cat}/K_m of 30 s^{-1} M^{-1}. For comparison, the corresponding parameters of the closely related TtPRODH (47% identical to DrPRODH) are as follows: k_{cat} = 13 s^{-1}, and K_m = 27 mM.[21] Those of the *E. coli* PutA are as follows: k_{cat} = 5.2 s^{-1}, and K_m = 42 mM.[27] Thus, the K_m for proline of DrPRODH is higher than expected. The kinetic parameters were also determined using CoQ1 as the variable substrate at fixed proline concentration. These values are as follows: k_{cat} = 14 s^{-1}, and K_m = 155 μM. The corresponding values for TtPRODH are not available. Those of the *E. coli* PutA are as follows: k_{cat} = 3.4 s^{-1}, and K_m = 110 μM.[27] Finally, THFA was found to inhibit DrPRODH competitively with proline. The estimated K_I value of 38 mM is >10 times higher than those of TtPRODH (1 mM[21]) and PutA (1.6 mM[27]). These results suggest that the affinity of DrPRODH for proline is atypically low.

Catalytic activity is severely impaired in mutants G63A and E64A (Table 2). Using proline as the varying substrate, k_{cat} values of 0.08 and 0.055 s^{-1} were obtained for G63A and E64A, respectively, which are >100 times lower than that of DrPRODH. The catalytic efficiencies of G63A and E64A for proline are 140- and 27-fold lower than that of DrPRODH, respectively. Using CoQ1 as the varying substrate, the k_{cat} values are 0.043 and 0.046 s^{-1} for G63A and E64A, respectively, which are 300-fold lower than that of DrPRODH. The efficiencies of the mutants for CoQ1 are 60-fold lower than that of DrPRODH. In summary, the kinetic analysis of G63A and E64A confirms the significance of the conserved sequence motif and is consistent with the structures, which suggest that Gly63 is important for the flexibility of the β1−α1 loop and Glu64 is important for stabilizing the closed active site.

DISCUSSION

The DrPRODH structures provide new information about the conformations populated by monofunctional PRODHs during the reductive half-reaction (Figure 1B). In particular, the $DrPRODH_o$−THFA structure represents the E−S complex [state II (Figure 1B)]. The active site of the E−S complex is closed, and the substrate is buried. The tight packing within the complex is also observed in PutA86−669 (Figure 3B) and presumably helps align proline with the flavin for the hydride transfer. A water molecule is present in the E−S complex, which bridges conserved Tyr193 and the THFA heteroatom (N atom of proline). An analogous water molecule is also present in the PutA86−669−THFA complex (Figure 3B), suggesting that it is conserved in the PRODH superfamily. It is tempting to speculate that this water molecule hydrolyzes P5C to GSA. If so, the hydrolysis reaction occurs within the active site rather than in solution as implied in Figure 1A and most biochemistry textbooks and literature articles on proline catabolism.

The E−S complexes of DrPRODH and PutA86−669 are very similar (Figure 3B). In both cases, the inhibitor is completely buried between the *si* face of the FAD and α8. The enzyme−inhibitor interactions and ion pair gate conformation are virtually identical in the two structures. Thus, substrate recognition is highly conserved in the PRODH superfamily. The only notable difference involves the conserved glutamate of α8 (Glu295 of DrPRODH and Glu559 of PutA). The different orientations of this side chain seem to be related to the different conformations of the FAD adenosine groups. In DrPRODH, the adenine ring packs against α8 and forms a hydrogen bond with Glu295 (Figure 3B). This interaction is not possible in PutA because of the markedly different location of the adenosine (Figure 5A), which is caused by the presence of an extra α-helix in PutAs that is absent in monofunctional PRODHs.[21]

Given the sequence and structural conservation of the proline binding site, it is surprising that DrPRODH has a markedly lower substrate affinity than PutA and TtPRODH. One possibility is that the FAD ribityl plays a role in tuning substrate affinity. DrPRODH is unique in that two conformations of the ribityl are observed in the E−S complex, neither of which corresponds to that of the high-affinity PutA86−669−THFA complex, although conformation A is reminiscent of the flavin in the PutA86−669−THFA complex. It is possible that conformation B represents an inactive state

and that a conformational change is required to transform it to conformation A before hydride transfer occurs. If so, Glu295 may play a role in this transformation because it hydrogen bonds with the 3′-OH of conformation B (Figure 4A). Additional structures of PRODH−THFA complexes would shed light on this issue.

Comparison of the $DrPRODH_o$−THFA and $DrPRODH_r$ structures provides insight into conformational changes that occur upon flavin reduction and product release (state II to state IV in Figure 1B). These include severe bending of the isoalloxazine, dihedral rotation of the ribityl chain, shifting of α8, reconfiguration of the β1−α1 loop, rupture of the conserved Arg291−Glu64 ion pair, and disordering of Glu295.

The structures suggest a scenario for how the enzyme moves from state II to state IV of the reductive half-reaction. The butterfly bending of the isoalloxazine appears to initiate a cascade of events that leads to product release. Bending of the ring system pushes the N5−N10 axis of the flavin toward the newly formed product, creating steric clash in the highly crowded active site. The shifting of α8 and rupture of the Arg291−Glu64 ion pair alleviate this clash, creating a large cavity that presumably allows facile product dissociation.

The Arg291−Glu64 ion pair is a central player in the conformational changes observed in DrPRODH. Because it is formed in the closed E−S complex and broken in the ligand-free state, the ion pair appears to function as the active site gate. Because the ion pairing residues are identically conserved in monofunctional PRODHs and PutAs, we suggest that the gate is a universal aspect of PRODH catalysis.

Whereas the ion pair gate opens to the bulk medium in DrPRODH, the gate of PutA separates the proline binding site from a large, internal cavity that traverses 41 Å to the P5CDH active site.[20] This cavity serves as a conduit through which P5C/GSA is channeled to the P5CDH active site. In the structure of full-length *B. japonicum* PutA, the gate is closed and a sulfate ion is bound in the PRODH active site. A structure of this enzyme with the proline site empty is not available, but on the basis of the DrPRODH structures, we predict that reduction of the FAD in PutA opens the gate, allowing P5C/GSA to enter the substrate channeling cavity. Curiously, dithionite reduction of the crystalline PutA86−669−THFA complex does not break the ion pair, although the flavin conformation is altered as in $DrPRODH_r$.[28] It is possible that crystal contacts inhibit rupture of the gate in crystalline PutA86−669. Clearly, new structures of full-length PutAs are needed to understand how the ion pair gate functions in PutA.

The structural changes observed in DrPRODH perhaps also provide insight into functional switching of trifunctional PutAs. Trifunctional PutA is a type of flavin switch protein that serves as a transcriptional repressor of the *put* regulon in addition to having PRODH and P5CDH catalytic activities.[31] How trifunctional PutA switches from being a DNA-bound transcriptional repressor to membrane-associated bifunctional enzyme (also known as functional switching) is a major question in PutA biochemistry. Recent rapid reaction kinetic measurements of the paradigmatic trifunctional PutA from *E. coli* revealed an isomerization step that occurs after reduction of FAD, and this step was proposed to report on flavin-dependent, global conformational changes that drive functional switching.[32] Because rupture of the ion pair gate and movement of α8 occur after flavin reduction in DrPRODH, it is possible that analogous changes are also part of functional switching. Because α8 and the β1−α1 loop contact other structural elements in PutA that are absent in monofunctional PRODHs, rupture of the ion pair and shifting of α8 in trifunctional PutA could help initiate a cascade of events that eventually leads to a larger, more global isomerization of the protein that unveils a high-affinity membrane association domain.

Finally, although it was not possible to crystallize DrPRODH in the absence of THFA, presumably the active site of the oxidized enzyme is open prior to substrate binding (state I in Figure 1B). Indeed, this is true for TtPRODH. The structure of oxidized, ligand-free TtPRODH resembles $DrPRODH_r$ in that the ion pair gate is open and α8 is shifted away from the isoalloxazine (Figure 2B). In fact, the shift of α8 in TtPRODH is 1.3 Å larger than that of $DrPRODH_r$ (Figure 2B). Whether substrate binding to the open enzyme induces closure of the gate (induced fit) or the substrate binds to closedlike conformations that arise from thermal fluctuations (conformational selection) remains to be determined. However, the large conformational changes that are required to form the closed E−S complex seem to favor conformational selection as a plausible mechanism for substrate binding.[33]

■ ASSOCIATED CONTENT

Supporting Information

Electron density evidence for dual FAD conformations in the $DrPRODH_o$−THFA complex (Figure S1). This material is available free of charge via the Internet at http://pubs.acs.org.

Accession Codes

Atomic coordinates and structure factors have been deposited in the Protein Data Bank as entries 4H6Q ($DrPRODH_o$−THFA) and 4H6R ($DrPRODH_r$).

■ AUTHOR INFORMATION

Corresponding Author

*Department of Chemistry, University of Missouri—Columbia, Columbia, MO 65211. Phone: (573) 884-1280. Fax: (573) 882-2754. E-mail: tannerjj@missouri.edu.

Funding

Research reported in this publication was supported by the National Institute of General Medical Sciences of the National Institutes of Health via Grant GM065546.

Notes

The authors declare no competing financial interest.

■ ACKNOWLEDGMENTS

We thank Drs. Jonathan Schuermann and Jay Nix for help with X-ray data collection and processing. We thank Dr. Ray Stevens and the Joint Center for Structural Genomics for providing the DrPRODH clone and Dr. Christopher Hill for providing the pKA8H plasmid. Part of this research was performed at the Advanced Light Source. The Advanced Light Source is supported by the Director, Office of Science, Office of Basic Energy Sciences, of the U.S. Department of Energy under Contract DE-AC02-05CH11231. This work is based upon research conducted at the Advanced Photon Source on the Northeastern Collaborative Access Team beamlines, which are supported by Grant RR-15301 from the National Center for Research Resources at the National Institutes of Health. Use of the Advanced Photon Source, an Office of Science User Facility operated for the U.S. Department of Energy (DOE) Office of Science by Argonne National Laboratory, was supported by the U.S. DOE under Contract DE-AC02-06CH11357.

■ ABBREVIATIONS

PRODH, proline dehydrogenase; P5C, 1-pyrroline-5-carboxylate; GSA, glutamate semialdehyde; P5CDH, 1-pyrroline-5-carboxylate dehydrogenase; POX, human proline oxidase; TtPRODH, proline dehydrogenase from *T. thermophilus*; PutA, proline utilization A; DrPRODH, proline dehydrogenase from *D. radiodurans* R1; $DrPRODH_o$, oxidized proline dehydrogenase from *D. radiodurans* R1; $DrPRODH_r$, reduced proline dehydrogenase from *D. radiodurans* R1; THFA, L-tetrahydrofuroic acid; CoQ1, coenzyme Q1; TEVP, tobacco etch virus protease; PutA86−669, PRODH construct of *E. coli* PutA containing residues 86−669.

■ REFERENCES

(1) Adams, E., and Frank, L. (1980) Metabolism of proline and the hydroxyprolines. *Annu. Rev. Biochem. 49*, 1005−1061.

(2) Tanner, J. J. (2008) Structural biology of proline catabolism. *Amino Acids 35*, 719−730.

(3) Singh, R. K., and Tanner, J. J. (2012) Unique Structural Features and Sequence Motifs of Proline Utilization A (PutA). *Front. Biosci. 17*, 556−568.

(4) Phang, J. M. (1985) The regulatory functions of proline and pyrroline-5-carboxylic acid. *Curr. Top. Cell. Regul. 25*, 92−132.

(5) Phang, J. M., Donald, S. P., Pandhare, J., and Liu, Y. (2008) The metabolism of proline, a stress substrate, modulates carcinogenic pathways. *Amino Acids 35*, 681−690.

(6) Donald, S. P., Sun, X. Y., Hu, C. A., Yu, J., Mei, J. M., Valle, D., and Phang, J. M. (2001) Proline oxidase, encoded by p53-induced gene-6, catalyzes the generation of proline-dependent reactive oxygen species. *Cancer Res. 61*, 1810−1815.

(7) Hu, C. A., Donald, S. P., Yu, J., Lin, W. W., Liu, Z., Steel, G., Obie, C., Valle, D., and Phang, J. M. (2007) Overexpression of proline oxidase induces proline-dependent and mitochondria-mediated apoptosis. *Mol. Cell. Biochem. 295*, 85−92.

(8) Liu, Y., Borchert, G. L., Surazynski, A., Hu, C. A., and Phang, J. M. (2006) Proline oxidase activates both intrinsic and extrinsic pathways for apoptosis: The role of ROS/superoxides, NFAT and MEK/ERK signaling. *Oncogene 25*, 5640−5647.

(9) Pandhare, J., Cooper, S. K., and Phang, J. M. (2006) Proline oxidase, a proapoptotic gene, is induced by troglitazone: Evidence for both peroxisome proliferator-activated receptor γ-dependent and -independent mechanisms. *J. Biol. Chem. 281*, 2044−2052.

(10) Cooper, S. K., Pandhare, J., Donald, S. P., and Phang, J. M. (2008) A novel function for hydroxyproline oxidase in apoptosis through generation of reactive oxygen species. *J. Biol. Chem. 283*, 10485−10492.

(11) Phang, J. M., Pandhare, J., and Liu, Y. (2008) The metabolism of proline as microenvironmental stress substrate. *J. Nutr. 138*, 2008S−2015S.

(12) Phang, J. M., Pandhare, J., Zabirnyk, O., and Liu, Y. (2008) PPARγ and Proline Oxidase in Cancer. *PPAR Res. 2008*, 542694.

(13) Liu, Y., Borchert, G. L., Donald, S. P., Diwan, B. A., Anver, M., and Phang, J. M. (2009) Proline oxidase functions as a mitochondrial tumor suppressor in human cancers. *Cancer Res. 69*, 6414−6422.

(14) Liu, Y., Borchert, G. L., Donald, S. P., Surazynski, A., Hu, C. A., Weydert, C. J., Oberley, L. W., and Phang, J. M. (2005) MnSOD inhibits proline oxidase-induced apoptosis in colorectal cancer cells. *Carcinogenesis 26*, 1335−1342.

(15) Phang, J. M., Hu, C. A., and Valle, D. (2001) Disorders of proline and hydroxyproline metabolism. In *Metabolic and molecular basis of inherited disease* (Scriver, C. R., Beaudet, A. L., Sly, W. S., and Valle, D., Eds.) pp 1821−1838, McGraw-Hill, New York.

(16) Willis, A., Bender, H. U., Steel, G., and Valle, D. (2008) PRODH variants and risk for schizophrenia. *Amino Acids 35*, 673−679.

(17) Lee, Y. H., Nadaraia, S., Gu, D., Becker, D. F., and Tanner, J. J. (2003) Structure of the proline dehydrogenase domain of the multifunctional PutA flavoprotein. *Nat. Struct. Biol. 10*, 109−114.

(18) Zhang, M., White, T. A., Schuermann, J. P., Baban, B. A., Becker, D. F., and Tanner, J. J. (2004) Structures of the *Escherichia coli* PutA proline dehydrogenase domain in complex with competitive inhibitors. *Biochemistry 43*, 12539−12548.

(19) Ostrander, E. L., Larson, J. D., Schuermann, J. P., and Tanner, J. J. (2009) A conserved active site tyrosine residue of proline dehydrogenase helps enforce the preference for proline over hydroxyproline as the substrate. *Biochemistry 48*, 951−959.

(20) Srivastava, D., Schuermann, J. P., White, T. A., Krishnan, N., Sanyal, N., Hura, G. L., Tan, A., Henzl, M. T., Becker, D. F., and Tanner, J. J. (2010) Crystal structure of the bifunctional proline utilization A flavoenzyme from *Bradyrhizobium japonicum*. *Proc. Natl. Acad. Sci. U.S.A. 107*, 2878−2883.

(21) White, T. A., Krishnan, N., Becker, D. F., and Tanner, J. J. (2007) Structure and kinetics of monofunctional proline dehydrogenase from *Thermus thermophilus*. *J. Biol. Chem. 282*, 14316−14327.

(22) Kabsch, W. (2010) XDS. *Acta Crystallogr. D66*, 125−132.

(23) Evans, P. (2006) Scaling and assessment of data quality. *Acta Crystallogr. D62*, 72−82.

(24) Vagin, A., and Teplyakov, A. (1997) MOLREP: An automated program for molecular replacement. *J. Appl. Crystallogr. 30*, 1022−1025.

(25) Emsley, P., and Cowtan, K. (2004) Coot: Model-building tools for molecular graphics. *Acta Crystallogr. D60*, 2126−2132.

(26) Adams, P. D., Afonine, P. V., Bunkoczi, G., Chen, V. B., Davis, I. W., Echols, N., Headd, J. J., Hung, L. W., Kapral, G. J., Grosse-Kunstleve, R. W., McCoy, A. J., Moriarty, N. W., Oeffner, R., Read, R. J., Richardson, D. C., Richardson, J. S., Terwilliger, T. C., and Zwart, P. H. (2010) PHENIX: A comprehensive Python-based system for macromolecular structure solution. *Acta Crystallogr. D66*, 213−221.

(27) Moxley, M. A., Tanner, J. J., and Becker, D. F. (2011) Steady-state kinetic mechanism of the proline:ubiquinone oxidoreductase activity of proline utilization A (PutA) from *Escherichia coli*. *Arch. Biochem. Biophys. 516*, 113−120.

(28) Zhang, W., Zhang, M., Zhu, W., Zhou, Y., Wanduragala, S., Rewinkel, D., Tanner, J. J., and Becker, D. F. (2007) Redox-induced changes in flavin structure and roles of flavin N(5) and the ribityl 2′-OH group in regulating PutA-membrane binding. *Biochemistry 46*, 483−491.

(29) White, T. A., Johnson, W. H., Jr., Whitman, C. P., and Tanner, J. J. (2008) Structural basis for the inactivation of *Thermus thermophilus* proline dehydrogenase by N-propargylglycine. *Biochemistry 47*, 5573−5580.

(30) Srivastava, D., Zhu, W., Johnson, W. H., Jr., Whitman, C. P., Becker, D. F., and Tanner, J. J. (2010) The structure of the proline utilization a proline dehydrogenase domain inactivated by N-propargylglycine provides insight into conformational changes induced by substrate binding and flavin reduction. *Biochemistry 49*, 560−569.

(31) Becker, D. F., Zhu, W., and Moxley, M. A. (2011) Flavin redox switching of protein functions. *Antioxid. Redox Signaling 14*, 1079−1091.

(32) Moxley, M. A., and Becker, D. F. (2012) Rapid reaction kinetics of proline dehydrogenase in the multifunctional proline utilization A protein. *Biochemistry 51*, 511−520.

(33) Grant, B. J., Gorfe, A. A., and McCammon, J. A. (2010) Large conformational changes in proteins: Signaling and other functions. *Curr. Opin. Struct. Biol. 20*, 142−147.

(34) Engh, R. A., and Huber, R. (1991) Accurate bond and angle parameters for X-ray protein structure refinement. *Acta Crystallogr. A47*, 392−400.

(35) Lovell, S. C., Davis, I. W., Arendall, W. B., III, de Bakker, P. I., Word, J. M., Prisant, M. G., Richardson, J. S., and Richardson, D. C. (2003) Structure validation by Cα geometry: ϕ, ψ and Cβ deviation. *Proteins 50*, 437−450.

(36) DeLano, W. L. (2002) *The PyMOL User's Manual*, DeLano Scientific, San Carlos, CA.